Journal of the Energy Institute xxx (2018) 1–11

Contents lists available at ScienceDirect

Journal of the Energy Institute

journal homepage: http://www.journals.elsevier.com/journal-of-the-energy-institute

The use of equilibrium thermodynamic models for the prediction of inorganic phase changes in the co-firing of wheat straw with El Cerrejon coal

P. Xing [a], L.I. Darvell [a], J.M. Jones [a], L. Ma [b], M. Pourkashanian [b], J. Szuhánszki [b], A. Williams [a, *]

[a] School of Chemical and Process Engineering, University of Leeds, Leeds, LS2 9JT, UK
[b] Energy Engineering Group, Department of Mechanical Engineering, University of Sheffield, Sheffield, S10 2TN, UK

ARTICLE INFO

Article history:
Received 12 September 2017
Received in revised form
13 February 2018
Accepted 19 February 2018
Available online xxx

Keywords:
Biomass
Coal
Co-firing
Ash composition

ABSTRACT

The combustion of pulverised coal in power stations results in slagging and fouling in the boiler section and this can be a more severe problem when co-fired with biomass, especially straw. Prediction of the effects of different combination of biomass and coal are helpful to the plant operators. Predictive software gives information about the onset and nature of the slag formed but often the results of these calculations have to be validated. This was undertaken in this work which gave a comparison of ash behaviour for coal (El Cerrejon) and wheat straw blends studied by ash fusion test, X-ray diffraction (XRD) and by using predictive software (FactSage). Ash prepared in the laboratory was also compared with ash produced in a 250 kW pilot-scale test furnace. The FactSage model showed good agreements with XRD data for the presence of inorganic phases with temperature, although it predicted some inorganic phases which are not detected in the XRD, particularly in low temperature ashes. Nevertheless, FactSage gave insight into liquid phase formation, more so than the ash fusion test, since it predicted the beginning of slag formation below the initial deformation temperature seen in the ash fusion test. For the coal, wheat straw and their blends, FactSage always predicted that slag formation is near to completion by the flow temperature observed in the ash fusion test.

1. Introduction

The combustion of pulverised coal in power stations results in slagging and fouling in the boiler section. This can reduce heat transfer, cause corrosion on the burner and the boiler tubes, and reduce gas flow. When biomass is co-fired with coal there are additional problems related due to the inorganic constituents in the biomass, particularly potassium. The mechanism for the formation of alkali-induced slagging and silicate melt-induced slagging is complex and difficult to predict [1–5]. Slagging is mainly generated by the deposit of molten fly ash from the high temperature radiant region in the furnace when it enters the cooler heat transfer regions of the boiler [4]. Fouling is always observed in the high temperature convection sections and is caused by ash condensation/deposition especially by sulphated ash [4]. In pulverised fuel power plants using high levels of biomass, the ash-related problems are increased because of the potassium in the biomass being released during combustion [4,5]. In a fluidized bed or grate furnaces, the high alkali and chlorine content of biomass combustion results in similar problems. The alkali-induced slagging commonly occurs on superheaters where the compact deposit reduces the heat transfer efficiency [2]. Furthermore, the alkali/chlorine compounds in the deposits contribute to corrosion, which may cause damage to the tubes [4,5], and in the case of a fluidised bed combustor can lead to formation of low temperature melting compounds which could lead to defluidisation [6]. The inorganic composition of different biomass can vary considerably [1,7]. Woody biomass has a low silicon content and low potassium but high calcium content; agricultural residues such as straw have high silica, high potassium and low calcium content. The release of potassium from biomass during combustion occurs in different forms, such as KCl for a biomass with a high content of both K and

* Corresponding author.
E-mail address: fueaw@leeds.ac.uk (A. Williams).

https://doi.org/10.1016/j.joei.2018.02.003

Cl, and as KOH for the biomass with a low content of Cl. K_2SO_4 is thought to form via gas phase reactions, particularly when co-firing with coal because of the sulphur present in the system.

These problems have been considered by a number of research groups. Of particular interest is the drop tube study by Wang et al. [8]. This provides evidence that the sulphates and especially the chlorides are the decisive species which result in ash deposits. In that study ash deposits were compared with different amounts of vaporised KCl and SO_2 released during biomass combustion. The initial SO_2 is oxidised to SO_3 which then reacts with KCl to give K_2SO_4 and $KHSO_4$, thus reducing the concentration of KCl in the gas phase. When the gas temperature decreases in the furnace, the alkali sulphates condense to produce aerosols of K_2SO_4 which form the deposits on the cooler surfaces of the boiler tubes [8–10]. Similar results were also observed in biomass fired power plants [1,9] where layers of deposits can be seen: the initial sticky layer of KCl and $K_3Na(SO_4)_2$ etc deposited as aerosols followed by a layer of captured of coarse particles with high Si and Al content which contribute to the deposit, and the process is repeated. And this problem is also found in gasification plants [10].

There has been some success in predicting the complex processes leading to ash formation based on equilibrium modelling using methods such as the minimisation of Gibbs Free Energy [11–14]. These have been developed into computer programs such as FactSage which computes the composition and phase of the ash [11]. These models are limited however by the accuracy of the thermodynamic data base and the range of species that can be examined. In order to evaluate the ash transformation reactions, the combustion temperature, the fuel composition and air input are required. The attainment of the equilibrium conditions is limited by the available residence time and furnace temperature.

The behaviour of ash from El Cerrejon coal and pine and their blends when used in a pf furnace has been previously examined in this way [12,13] as well as the influence of unburned carbon in the ash samples [14]. In this work the behaviour of the same coal with wheat straw, and in particular, the suitability of the FactSage code as an accurate prediction tool is examined. This is achieved by using experimental data using XRD (X-ray diffraction) to determine inorganic species present, and comparing this to those predicted by means of FactSage. It should also be noted that apart from the accuracy of the thermodynamic criteria used in the computation the residence time required to reach equilibrium conditions may involve other kinetic factors. The slag formed from the cooling of molten material, is for most coals based on silicates, the clays and the quartz in the original coal. In thermodynamic terms a glassy slag is not a material has reached equilibrium, since the time at high temperatures has been insufficient for crystallisation to occur to give the stable crystalline phases and this behaviour should be taken into account [15–17].

2. Methodologies

2.1. Sample preparation

The solid fuels selected were typical of fuels burned in large scale pulverised fuel power plants in Europe. They were a Colombian coal, El Cerrejon and a wheat straw. It should be noted that this is an interesting fuel combination in that the ash content of the El Cerrejon coal is very low for a power station coal, whilst the ash content of the wheat straw is quite high for a biomass. Their Proximate and Ultimate compositions are shown in Table 1; coal no. 1 was used for the laboratory measurements and previously used [13] and coal no. 2 used for the pilot-scale test furnace studies described later. The oxide contents of ash for the coal [13] and the straw [14] have been published previously. The sample designations are given in Table 2.

Ash samples were prepared in two ways. Firstly, because of the presence of impurities in a large-scale furnace, especially unburned carbon, we have simplified the process by making ash sample from the fuels under laboratory conditions. Secondly, we have used ash produced by a pilot-scale test furnace. Laboratory ash samples were prepared from the fuels firstly reducing their size to <2 mm (top size) using a Retzch cutting mill. Then they were ashed in porcelain crucibles in an electric furnace at temperatures of 550 °C and 800 °C (British Standard DD CEN/TS 15370-1:2006). All samples were initially reduced to ash at the lower temperature. The samples were subsequently subject to higher temperatures to minimise residual carbon, the presence of which was apparent from visual appearance (dark grey-black colour) as previously described [14]. The resulting ashes were manually ground and sieved to <106 μm. Ash fusion data was obtained as previously described [13] and are listed in Table 2.

Ash samples were also obtained from a nominal 250 kW pilot-scale test furnace sited at the UKCCSRC PACT facilities which have been previously described [18]. The fuel flow rate was 200 kW (24.4 kg/h), and the primary and secondary/tertiary air flow rates were 60.1 ± 0.2 kg/h and 244 ± 1 kg/h respectively. The temperature profile indicated a maximum temperature of 1300 °C in the initial 500 mm which steadily decreased to 900 °C at 3500 mm where the bottom and fly ash left the combustion chamber. In these experiments El Cerrejon coal no. 2 was used and was pre-milled in the UK prior to the experimental investigation (90% < 210 μm, mean diameter = 125 μm). Samples of ash from the combusted fuels were collected at three sampling points in the furnace and the designations of samples of ash are given in Table 3. Fly ash was collected from a candle filter in the exit gases (designated Collection Point 1) and this designated as CFA1; ash collected

Table 1
Proximate and ultimate analyses of fuels used (wt %).

	Wheat straw	El Cerrejon coal no. 1	El Cerrejon coal no. 2
% Moisture	8.63	6.63	8.13
% Ash	6.48	3.83	3.42
% Fixed Carbon	8.46	41.55	49.16
% Volatile matter	76.42	47.99	39.30
% C	47.45	75.94	79.08
% H	5.53	4.26	4.21
% N	0.58	1.76	1.43
% S	<0.03	0.64	0.32
% Cl	<0.3	<0.3	<0.3

Please cite this article in press as: P. Xing, et al., The use of equilibrium thermodynamic models for the prediction of inorganic phase changes in the co-firing of wheat straw with El Cerrejon coal, Journal of the Energy Institute (2018), https://doi.org/10.1016/j.joei.2018.02.003

Table 2
Ash sample designations and preparation conditions, together with ash fusion characteristic temperatures and slagging indices.

	Sample	Ashing temperature	SST °C	IDT °C	HT °C	FT °C	Fs °C	B/A
PCC1	100% El Cerrejon coal no. 1 ash	550 °C	980	1195	1315	1330	1219	0.33
PCC2	100%El Cerrejon coal no. 1 ash	800 °C	1005	1205	1360	1375	1236	0.33
PCC3	100%El Cerrejon coal 2 ash	800 °C	1050	1210	1370	1380	1322	0.31
WS1	100% wheat straw ash	550 °C	855	925	1105	1165	961	0.50
WS2	100% wheat straw ash	800 °C	N/A	N/A	N/A	N/A	N/A	N/A
BWCA82	Blended fuels: 80% wheat straw/20% coal, then ashed	550 °C	815	1010	1195	1225	1047	0.49
BWCA55	Blended fuels: 50% wheat straw/50% coal, then ashed	550 °C	860	1150	1245	1280	1169	0.42
BWCA28	Blended fuels: 20% wheat straw/80% coal, then ashed	550 °C	1080	1195	1295	1320	1215	0.34

at the furnace exit (Collection Point 2) is designated as CBA11, and bottom ash samples from the water tray beneath the furnace (Collection Point 3) is designated as CBA21. Samples from the test furnace contained unburned carbon, which was in amounts greater than typically found in a full scale furnace, and which were burned-off in a laboratory furnace at 800 °C, as described previously [14]. The ash fusion test results on the reheated ash are also given in Table 3.

2.2. XRD for inorganic phase studies

X-ray diffraction (XRD) was used to identify the inorganic composition of ash from coal, biomass and their mixtures. The analysis of ashes was conducted with an X-ray diffraction instrument (Bruker model D8) using Cu k_α radiation and a graphite monochromator (U = 35 kV, I = 35 mA). The XRD scans were performed between 2 and 70 2θ°, with a step size of 0.0330°/s and time of 1216s. DIFFRAC software was used for the evaluation of the data and the JCPDS database was used for data processing. The crystalline mineral species in the samples were determined by PANalytical's HighScore Plus software. The presence of a non-crystalline fraction in the slag/ash is indicated by a 'halo' seen in the diffraction patterns at the top of Figs. 1 and 2.

2.3. Equilibrium modelling: FactSage

Because of the limitations of the empirical indices in the prediction of slagging and fouling the equilibrium thermochemical model FactSage version 6.4 [11] was used to predict the formation of slags and to give insight into ash behavior as before [12,13]. The Proximate and Ultimate fuel data given in Table 1 together with the data for the oxides [13,14] were used as inputs. The FACTPS and FTOxid thermodynamic databases [15] were used and all ideal gas, solid and liquid solutions were calculated from the stoichiometric equations. The reactions were assumed to take place at a pressure of 1 bar and an oxygen content of 6 mol% O_2, these conditions being typical for a combustion chamber using pulverized fuel. A temperature range from 500 to 1800 °C was chosen for the reactions between C, O, H, N, S, P, K_2O, Na_2O, SiO_2, CaO, Al_2O_3, Fe_2O_3, MgO, MnO, and TiO_2. It was recognized that equilibrium cannot be reached at the lower temperatures in practice but the results are indicative of the situation under laboratory conditions.

3. Results and discussions

3.1. Inorganic composition of ash

The XRD analysis results are shown in Figs. 1 and 2. They show the compositions of El Cerrejon coal ash, wheat straw ashes and ashes prepared under different conditions in comparison to XRD patterns for identified inorganic species. Fig. 1 shows (a) El Cerrejon coal ash at 800 °C (PCC3-800 °C), (b) wheat straw at 550 °C (WS1-550 °C), and (c) wheat straw ash at 800 °C (WS2-800 °C). In Fig. 2 (a) to (c) analyses are given of ash compositions from El Cerrejon coal and mixtures with wheat straw of 20, 50 and 80% respectively, (BWC28, BWCA55 and BWCA82 as designated in Table 2.).

The crystalline mineral species in all the samples studied are listed in Tables 4 and 5. In Table 4 data resulting from the XRD analyses are given for wheat straw and El Cerrejon coal. It should be noted that all of the wheat straw ashes determined at 550 °C showed the presence of unburned carbon but this was not the case in the 800 °C biomass ashes. Furthermore the biomass ashes heated to 800 °C showed only slight changes in inorganic composition compared to the low temperature ashes as shown in Table 4.

Table 5 gives the species present for the inorganic species as determined by XRD for the biomass and coal (co-firing) mixtures. With an increasing ratio of wheat straw, the co-firing ash shows decreasing Fe, Al and Ti compounds and increasing amounts of P, K and Ca

Table 3
Designation of Pilot-scale furnace ash and retreated ash.

Original sampled ash	Retreated ash	Retreating temp	Ash fusion characteristics and slagging indices of reheated ashes					
			SST °C	IDT °C	HT °C	FT °C	Fs °C	B/A
Collection point 1 CFA1	CFA2	800 °C	980	1195	1315	1330	1219	0.33
Collection point 2 CBA11	CBA12	800 °C	1005	1205	1360	1375	1236	0.33
Collection point 3 CBA21	CBA22	800 °C		1210	1370	1380	1322	0.31

Please cite this article in press as: P. Xing, et al., The use of equilibrium thermodynamic models for the prediction of inorganic phase changes in the co-firing of wheat straw with El Cerrejon coal, Journal of the Energy Institute (2018), https://doi.org/10.1016/j.joei.2018.02.003

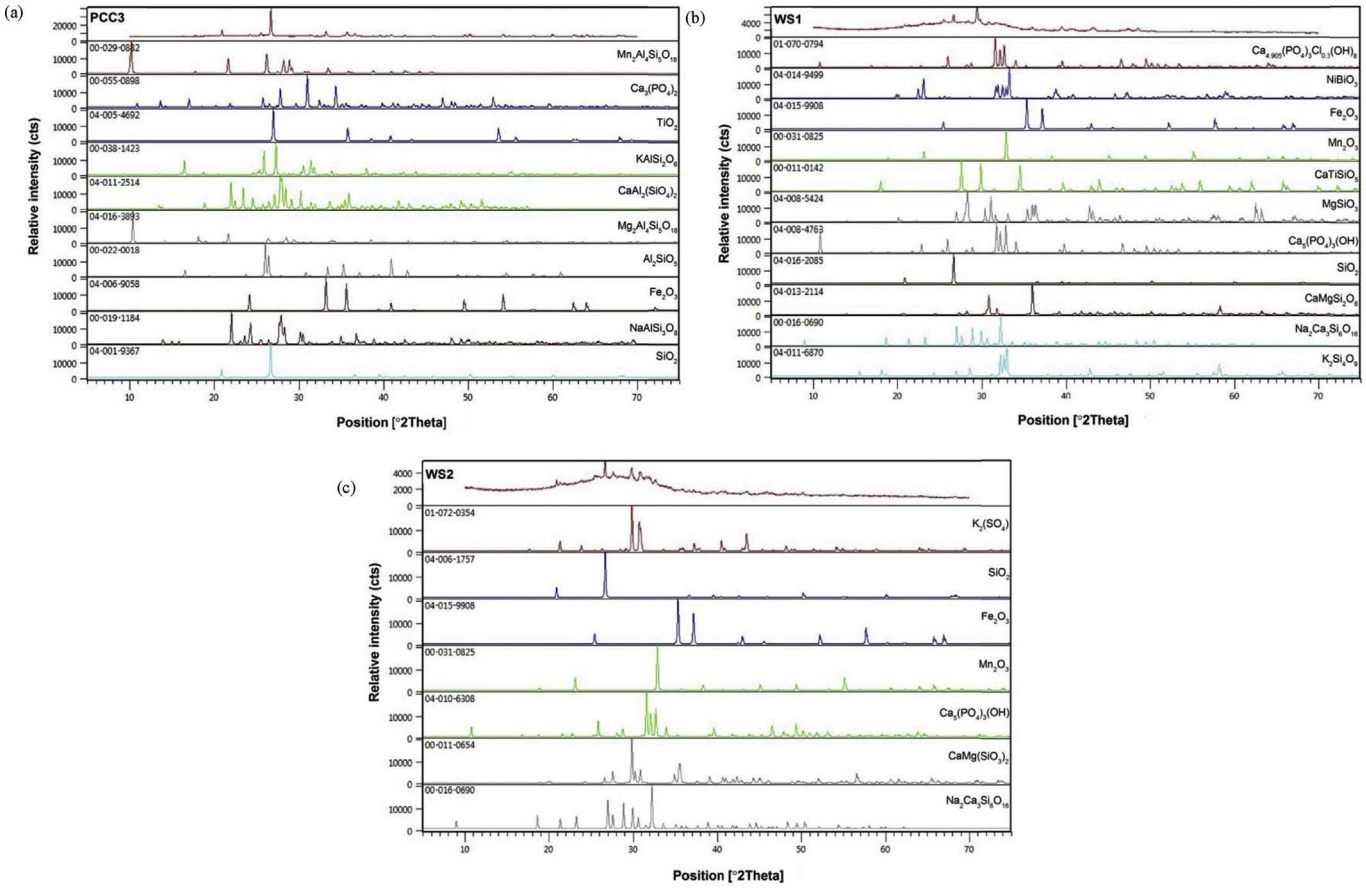

Fig. 1. Ash composition of (a) El Cerrejon no. 2 coal ash at 800 °C (PCC3), (b) wheat straw at 550 °C (WS1), and (c) wheat straw ash at 800 °C (WS2).

compounds. At 80% wheat straw, the mix of inorganic phases contains some of those seen in pure wheat straw ash (e.g. $CaMgSi_2O_6$, $Ca_5HO_{13}P_3$), but some are different due to interaction with the coal ash components, particularly K_2SO_4.

It is interesting to compare with pine ash which was studied previously [13] and where the dominant phosphorus compounds present decomposed; $Ca_{10}(PO_4)_6O$ decomposed to $Ca_5(PO_4)_3(OH)$ as the ashing temperature increased. The pine ashes contained higher Ca and P compounds and lower Si and Al compounds than the wheat straw ash studied here. Pine ash showed a greater tendency to change composition with increasing ashing temperature than wheat straw ashes. In both biomass-coal combinations, the dominant inorganic oxides Si, Fe, Al and Ti compounds decrease with increasing biomass ratio. In contrast, the P compounds, K compounds and Ca compounds increase. When the fuel/biomass ratio is 50/50, all the amounts of the inorganic compounds are intermediate between the extremes and thus the composition shows the greatest variety.

Samples of ash from the pilot-scale test furnace were prepared at a temperature of 800 °C and the XRD results of their composition are given in Table 6. The XRD patterns are generally simpler for the pure coal ash from the pilot-scale facility, compared to the coal-wheat straw ashes prepared in the laboratory. Also, there was interference from the carbon-in-ash, although this was eliminated by reheating the ash at 800 °C.

3.2. Thermal equilibrium model

Fig. 3 shows the predicted mass fraction of slag for a specific blend at a specified temperature, each bar represents a temperature for a particular blend. Also plotted on this figure are the lower and upper limits of the measured deformation temperature ranges, assumed to be represented as the lowest softening temperature (SST) and highest deformation temperature (DT) measured for each El Cerrejon coal 2 and Wheat straw blends or pure fuel; the solid and dashed line join these points to give an estimated region for where slagging is observed to occur experimentally. The pure wheat straw is predicted to be the most slagging at low temperature (i.e. has the largest change in slag mass fraction between 500 °C and 700 °C) while the pure El Cerrejon coal 2 and 80% coal blends are predicted to be the least slagging in this temperature range. The 50/50 blends are intermediate and have the largest change in slag mass fraction between 700 °C and 800 °C.

In the case of pure wheat straw ash, FactSage predicts slag generated from 500 °C, about 65% slag at 900 °C (near the experimental DT) and this increases to 75% at 1100 °C (HT is around 1100 °C), so the results predict slag at temperature close to the measured values. However the total amount of predicted slag is much higher at low temperature for the straw compared to the coal as seen in Fig. 3. Figs. 4–8 show the chemical composition of the predicted species calculated using FactSage for the fuels and fuel blends with different ratios, namely 100% El Cerrejon coal, 80% coal/20% wheat straw, 50/50 20/50 and 100% wheat straw.

Also shown in these figs are the DT HT FT and the Slagging Index Fs [19], which are listed in Tables 2 and 3, together with the ratio of basic to acid oxides in the ash. The Slagging Index is based on the initial deformation temperature (DT) and hemisphere temperature (HT)

Please cite this article in press as: P. Xing, et al., The use of equilibrium thermodynamic models for the prediction of inorganic phase changes in the co-firing of wheat straw with El Cerrejon coal, Journal of the Energy Institute (2018), https://doi.org/10.1016/j.joei.2018.02.003

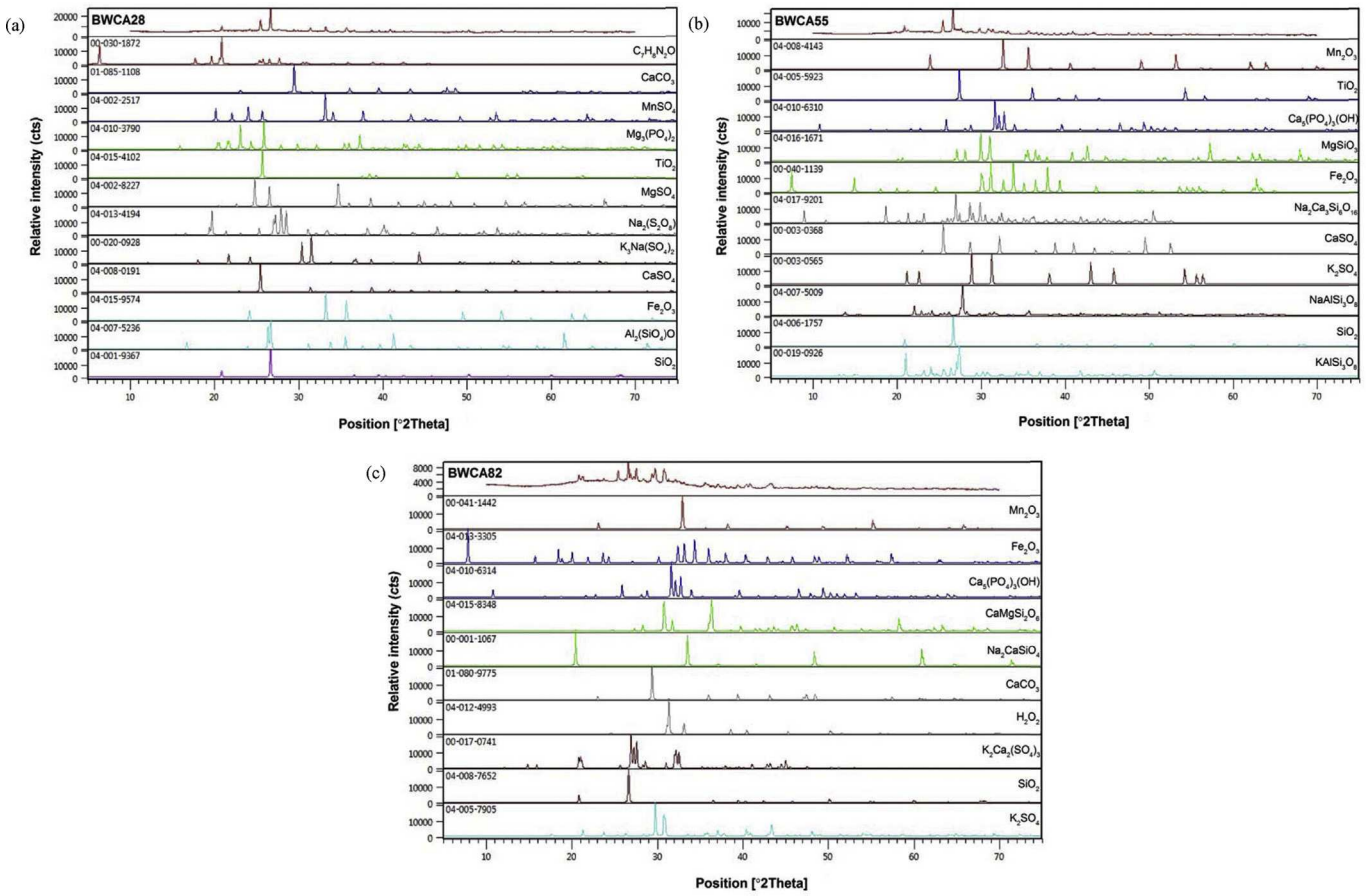

Fig. 2. (a) to (c). Ash analysis for El Cerrejon coal no. 2 and wheat straw blends: BAW28, BWCA55 and BWCA82 respectively.

observed during ash fusion tests, and it was also employed in this investigation to analyse the slagging propensity of the ash samples. The index is defined as:

$$FS = \{(4\,DT + HT)/5\}\ (^{\circ}C)$$

In Fig. 4 it is seen that the coal displays a lower weight of slag (about 16 g/kg of fuel) than the other mixtures and these are first seen to form at above 900 °C. In contrast, in the case of pure wheat straw ash shown in Fig. 8, FactSage predicts slag generated from 500 °C, about 65% slag at 900 °C (near the experimental Initial Deformation Temperature) and this increases to 75% at 1100 °C (Hemispherical Temperature is 1100 °C), so these results predict slag at temperatures close to the measured values. Additionally the Wheat straw (see Fig. 8) shows a high propensity of slag formation in terms of g/kg fuel, partially due to the higher ash of wheat straw compared to the coal, but also due to the change in composition. Modelling of the intermediate blends (Figs. 5–7) predicts intermediate slagging in terms of g/kg fuel and in terms of the temperature at which it is formed.

Comparison of the figs for 100% coal (Fig. 4) and 100% Wheat straw (Fig. 8) shows that the compositions during the phase changes become more complicated in the latter case. The coal slag is predicted as a mixture of Al_2O_3, FeO, $NaAlO_2$, SiO_2 and CaO, whereas the straw slag is mainly predicted as SiO_2, K_2O and CaO, and the blend slag as a mixture of Al_2O_3, FeO, $NaAlO_2$, K_2O, MgO and CaO. It is the role of the high concentration of K_2O in the straw mixtures that leads to formation of gaseous KCl, KOH and subsequent damage by deposition and corrosion.

Table 4
Comparison of inorganic phases identified in wheat straw ash and El Cerrejon coal ash by FactSage prediction and X-ray diffraction.

Wheat straw				El Cerrejon coal		
FactSage		XRD		FactSage		XRD
Phases identified	Temperature range (°C)	WS1(550 °C)	WS2(800 °C)	Phases identified	Temperature range (°C)	PCC3 (800 °C)
$K_2Si_4O_9$	500–600	✓		SiO_2	500–1200	✓
$Na_2Ca_3Si_6O_{16}$	500–1000	✓	✓	Al_2SiO_5	500–1100	✓
$CaMgSi_2O_6$	500–1200	✓	✓	$NaAlSi_3O_8$	600–900	✓
$Ca_5HO_{13}P_3$	500–1100	✓	✓	TiO_2	500–1200	✓
$MgSiO_3$	500–700	✓		$Mg_2Al_4Si_5O_{18}$	600–1200	✓
SiO_2	500–600, 900	✓	✓	$KAlSi_2O_6$	600–1200	✓
$CaSiTiO_5$	500–900	✓		$Mn_2Al_4Si_5O_{18}$	700–1100	✓
Mn_2O_3	500–800	✓	✓	$CaAl_2Si_2O_8$	800–1200	✓
Fe_2O_3	500–700	✓	✓	$Ca_3(PO_4)_2$	800–1000	✓

Please cite this article in press as: P. Xing, et al., The use of equilibrium thermodynamic models for the prediction of inorganic phase changes in the co-firing of wheat straw with El Cerrejon coal, Journal of the Energy Institute (2018), https://doi.org/10.1016/j.joei.2018.02.003

Table 5
Comparison of inorganic phases from El Cerrejon coal 2 and wheat straw co-firing by FactSage prediction and X-ray diffraction.

BWCA28			BWCA55			BWCA82		
FactSage		XRD	FactSage		XRD	FactSage		XRD
Phases identified	Temp range (°C)	550 °C	Phases identified	Temp range (°C)	550 °C	Phases identified	Temp range (°C)	550 °C
SiO_2	500–900	✓	$KAlSi_3O_8$	500	✓	$Na_2Ca_3Si_6O_{16}$	800–900	
Al_2SiO_5	500–700	✓	SiO_2	500–700	✓	$CaMgSi_2O_6$	800–1300	✓
Fe_2O_3	500–1200	✓	$NaAlSi_3O_8$	500–800	✓	K_2SO_4	800–900	✓
$CaSO_4$	500–700	✓	K_2SO_4	500–700	✓	$Ca_5HO_{13}P_3$	900–1100	✓
$K_3Na(SO_4)_2$	500	✓	$Na_2Ca_3Si_6O_{16}$	500–700	✓	Fe_2O_3	800	✓
Na_2SO_4	500		$CaSO_4$	500–800	✓	Mn_2O_3	800–900	✓
$MgSO_4$	500	✓	Fe_2O_3	500–1200	✓	$Ca_3Fe_2Si_3O_{12}$	900–1200	
TiO_2	500–1200	✓	$MgSiO_3$	500–600	✓	$CaSiO_3$	1000–1300	
$Mg_3P_2O_8$	500–700	✓	$Ca_5HO_{13}P_3$	500–1100	✓	$MnSiO_3$	1000–1100	
$MnSO_4$	500–600	✓	TiO_2	500	✓	$Ca_3(PO_4)_2$	1200–1600	
$NaAlSi_3O_8$	600–900		Mn_2O_3	500–1000	✓			

Table 6
The comparison of inorganic phases in Pilot Plant El Cerrejon 2 ash (identified by XRD) for ash heated to 800 °C and FactSage prediction for different temperature ranges.

Inorganic Phase	CFA1		CFA2		CBA11		CBA12		CBA21		CBA22	
	Fact Sage	XRD	Fact Sage	XRD	Fact Sage	XRD	Fact Sage	XRD	Fact Sage	XRD	Fact Sage	XRD
	Temp range (°C)	800 °C	Temp range (°C)	800 °C	Temp range (°C)	800 °C	Temp range (°C)	800 °C	Temp range (°C)	800 °C	Temp range (°C)	800 °C
SiO_2	500–1500	✓	500–1500	✓	500–1500	✓	500–1400	✓	500–1300	✓	500–1400	✓
$CaAl_2Si_2O_8$	500–1300	✓	500–1300	✓	500–1300	✓	500–1400	✓	500–1300	✓	500–1300	✓
Al_2SiO_5	500–1300	✓	500–1400	✓	500–1400	✓	500–1300	✓	500–1300	✓	500–1300	✓
$KAlSi_3O_8$	500		500	✓	500	✓	500	✓	–		500	✓
$KAlSi_2O_6$	600–1100		600–1100		600–1100		500–1400		–		600–1200	
Al_2O_3	–		–		1500		1500–1600		–		1500–1600	

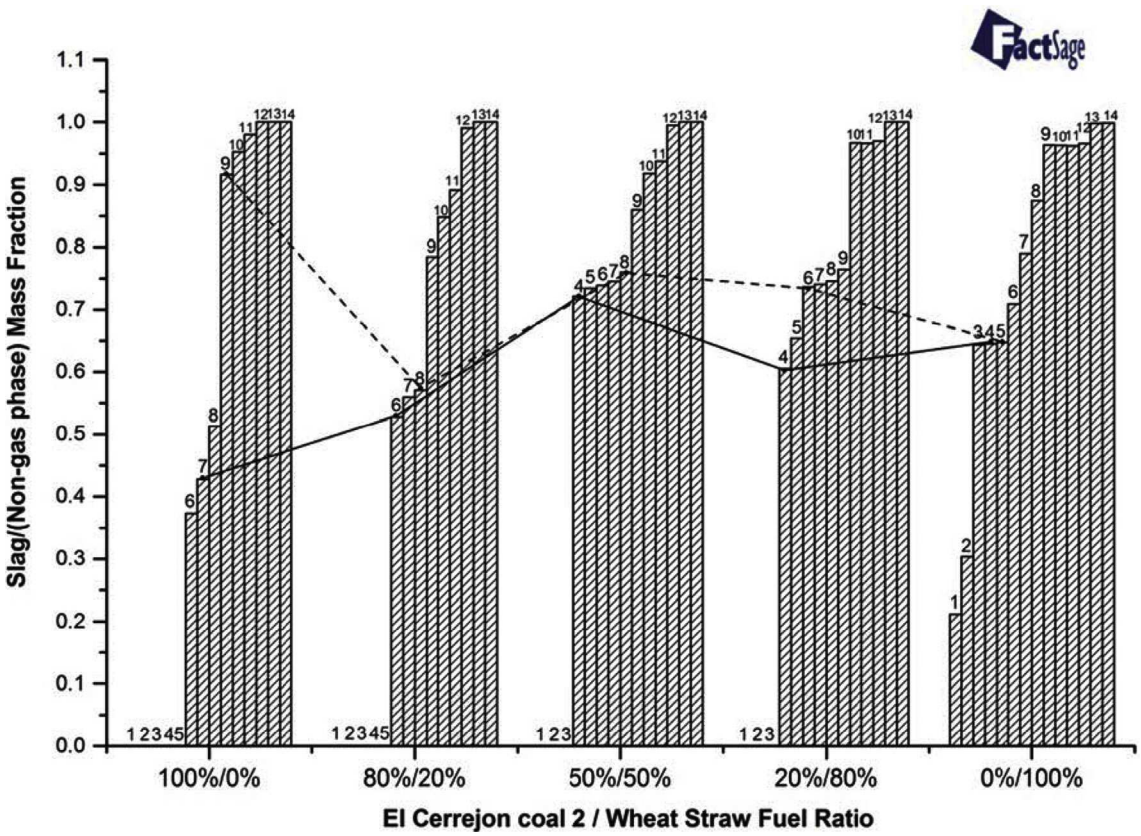

Fig. 3. The change of slag mass fraction in non-gas phase with increase in temperature for each El Cerrejon coal 2/wheat straw ratio as calculated by FactSage. Temperatures: 1, 500 °C; 2, 600 °C; 3, 700 °C; 4, 800 °C; 5, 900 °C; 6, 1000 °C; 7, 1100 °C; 8, 1200 °C; 9, 1300 °C; 10, 1400 °C; 11, 1500 °C; 12, 1600 °C; 13, 1700 °C; 14, 1800 °C. Solid and dashed line represents the lower and upper limits of the measured deformation temperature range (by ash fusion test) for the different blends.

Please cite this article in press as: P. Xing, et al., The use of equilibrium thermodynamic models for the prediction of inorganic phase changes in the co-firing of wheat straw with El Cerrejon coal, Journal of the Energy Institute (2018), https://doi.org/10.1016/j.joei.2018.02.003

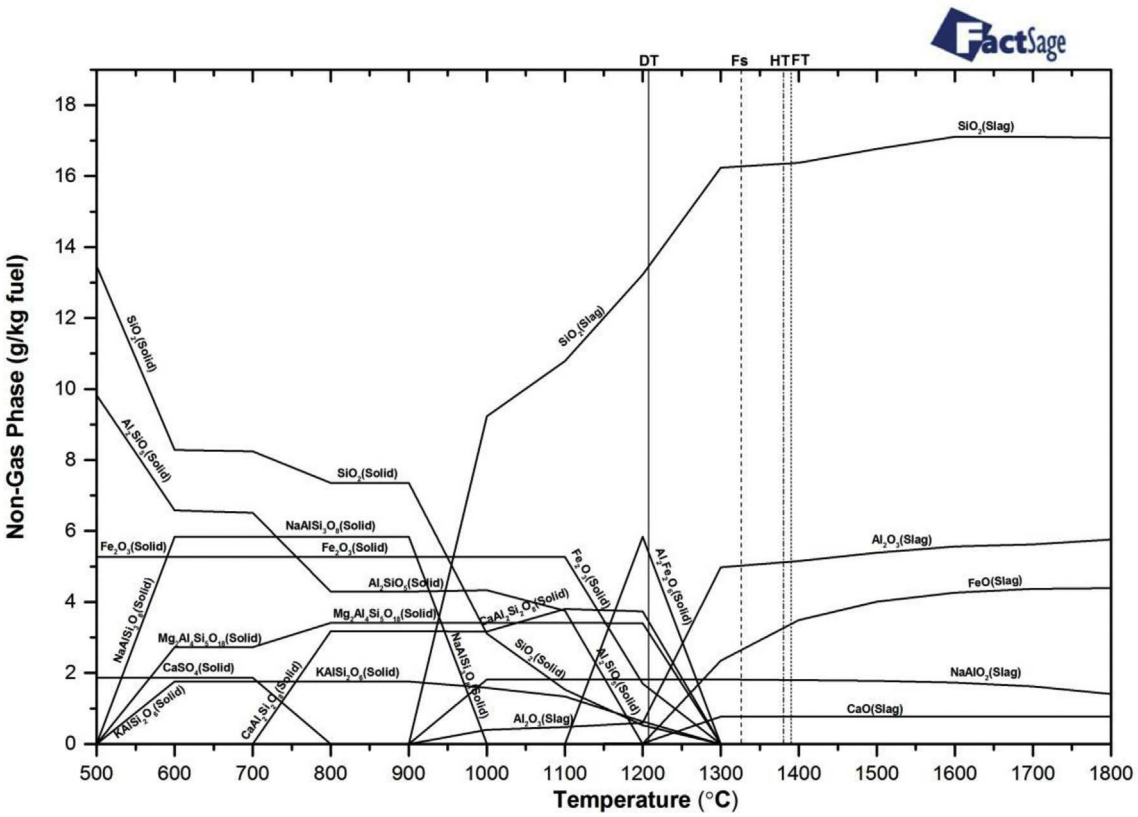

Fig. 4. Stable solid phases in equilibrium with the slag phase for 100% El Cerrejon coal (PCC3). The Initial Deformation Temperature (DT), the Hemispherical Temperature (HT), the Flow Temperature (FT) and the Slagging Index (Fs) are shown here and in the following figures.

As the wheat straw ratio increases in these five models the total non-gas phase content increases due to the higher ash content in the fuel. For the solid phase, as the coal ratio decreases from 100% to 80%, Al mainly exists in Al_2SiO_5 and decreases in the pure coal combustion after 500 °C. As the straw ratio increases, in the 50/50 mixture below 600 °C, most of the Al mainly exists as $KAlSi_3O_8$, and convert to $KAlSi_2O_6$, $NaAlSi_3O_8$ and K_2SO_4 as the temperature increases. After 800 °C all of these three compounds decompose into slag. As the straw ratio increases, the $CaSO_4$ content in the solid phase increases, and when the fuel ratio is 50/50, $Ca_5HO_{13}P_3$ is predicted in the solid phase. When the straw ratio increase to 80% and 100%, low Al content and high Ca content are present in the solid phase and $Na_2Ca_3Si_6O_{16}$, $CaMgSi_2O_6$, $Ca_5HO_{13}P_3$ and $Ca_3Fe_2Si_3O_{12}$ are predicted after 800 °C. The Si content increases with an increase in wheat straw ratio, and the higher ash content of straw contributes more Si species in the solid phase. In pure wheat straw, with an increase in temperature, $Na_2Ca_3Si_6O_{16}$, $CaMgSi_2O_8$ and $K_2Si_4O_8$ in the solid phase are decomposed to SiO_2, CaO and K_2O which are the main slagging components above 1000 °C. In the high coal ratio (from 100% to 80%), the main changes shown by plots in Figs. 5–7 are listed below:

$SiO_2(solid) + Al_2SiO_5(solid) + CaSO_4(solid) \rightarrow CaAl_2Si_2O_8(solid) + SO_2\ (gas)$ (800 °C–1200 °C)

$CaAl_2Si_2O_8(solid) \rightarrow SiO_2(slag) + Al_2O_3(slag) + CaO(slag)$ (1100 °C–1300 °C)

$NaAlSi_3O_8(solid) \rightarrow SiO_2(slag) + Al_2O_3(slag) + NaAlO_2(slag)$ (900 °C)

$Fe_2O_3(solid) + SiO_2(solid) + Al_2SiO_5(solid) \rightarrow Al_2Fe_2O_6(solid) + SiO_2(slag)$ (1100 °C–1200 °C)

$Al_2Fe_2O_6(solid) \rightarrow Al_2O_3(slag) + FeO(slag)$ (>1200 °C)

The most complicated phase change of 50/50 fuel ratio co-firing (BWCA55) in Fig. 6 can be described by the changes below:

$KAlSi_3O_8(solid) \rightarrow SiO_2(solid) + KAlSi_2O_6(solid)$ (600 °C)

$SiO_2(solid) + KAlSi_2O_6(solid) \rightarrow SiO_2(slag) + K_2O(slag) + Al_2O_3(slag)$ (800 °C)

$NaAlSi_3O_8(solid) \rightarrow SiO_2(slag) + Al_2O_3(slag) + NaAlO_2(slag)$ (900 °C)

$CaSO_4(solid) + MgSiO_3(solid) \rightarrow CaMgSi_2O_6(solid) + SO_2(gas)$ (900 °C)

$CaMgSi_2O_6(solid) \rightarrow CaO(slag) + SiO_2(slag) + MgO(slag)$ (>1200 °C)

$CaSO_4(solid) + SiO_2(solid) + Fe_2O_3(solid) \rightarrow Ca_3Fe_2Si_3O_{12}(solid) + SO_2(gas)$ (900 °C)

Please cite this article in press as: P. Xing, et al., The use of equilibrium thermodynamic models for the prediction of inorganic phase changes in the co-firing of wheat straw with El Cerrejon coal, Journal of the Energy Institute (2018), https://doi.org/10.1016/j.joei.2018.02.003

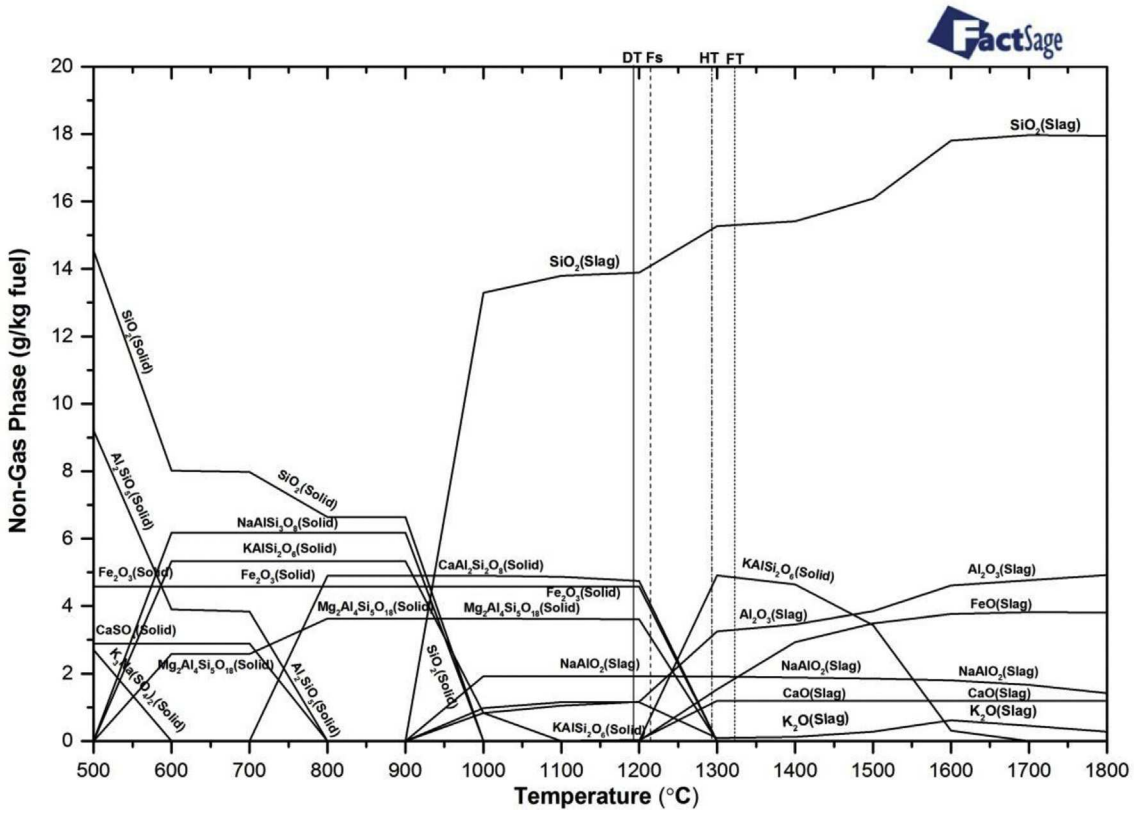

Fig. 5. Stable solid phases in equilibrium with the slag phase for 80% El Cerrejon coal no. 2 and 20% wheat straw co-combustion (BWCA28).

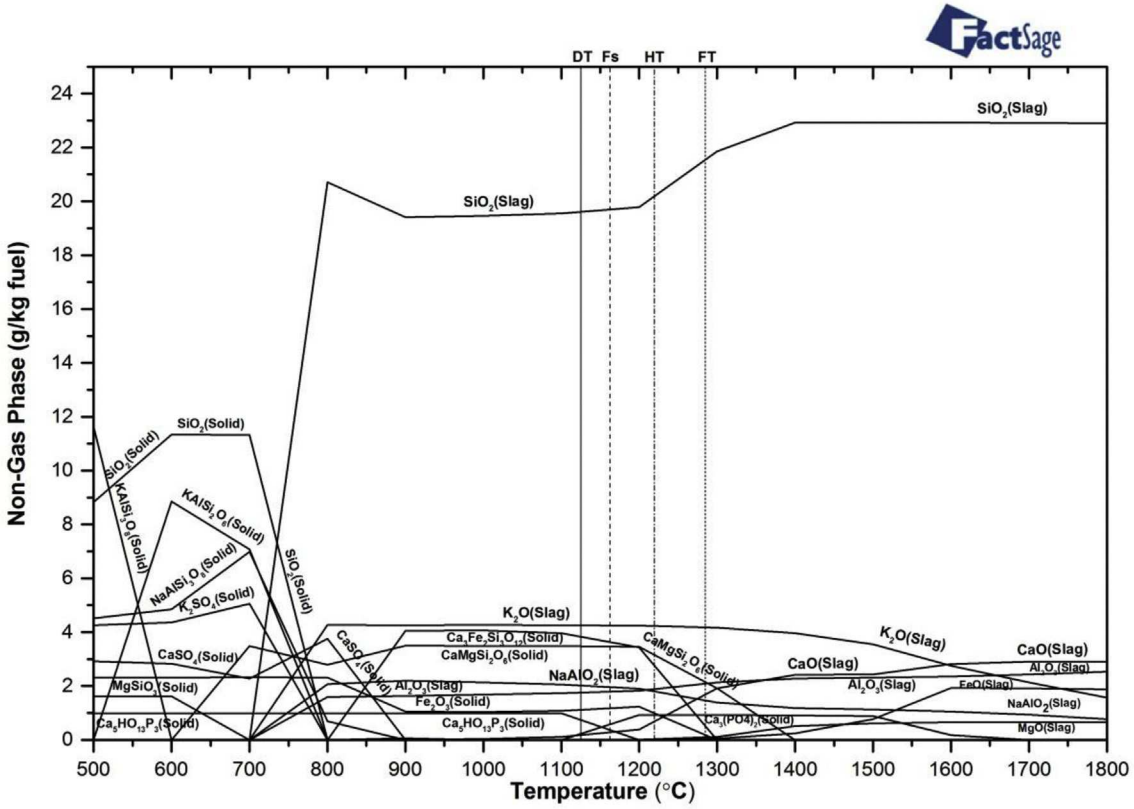

Fig. 6. Stable solid phases in equilibrium with the slag phase for 50% El Cerrejon coal 2 and 50% wheat straw co-combustion (BWCA55).

Please cite this article in press as: P. Xing, et al., The use of equilibrium thermodynamic models for the prediction of inorganic phase changes in the co-firing of wheat straw with El Cerrejon coal, Journal of the Energy Institute (2018), https://doi.org/10.1016/j.joei.2018.02.003

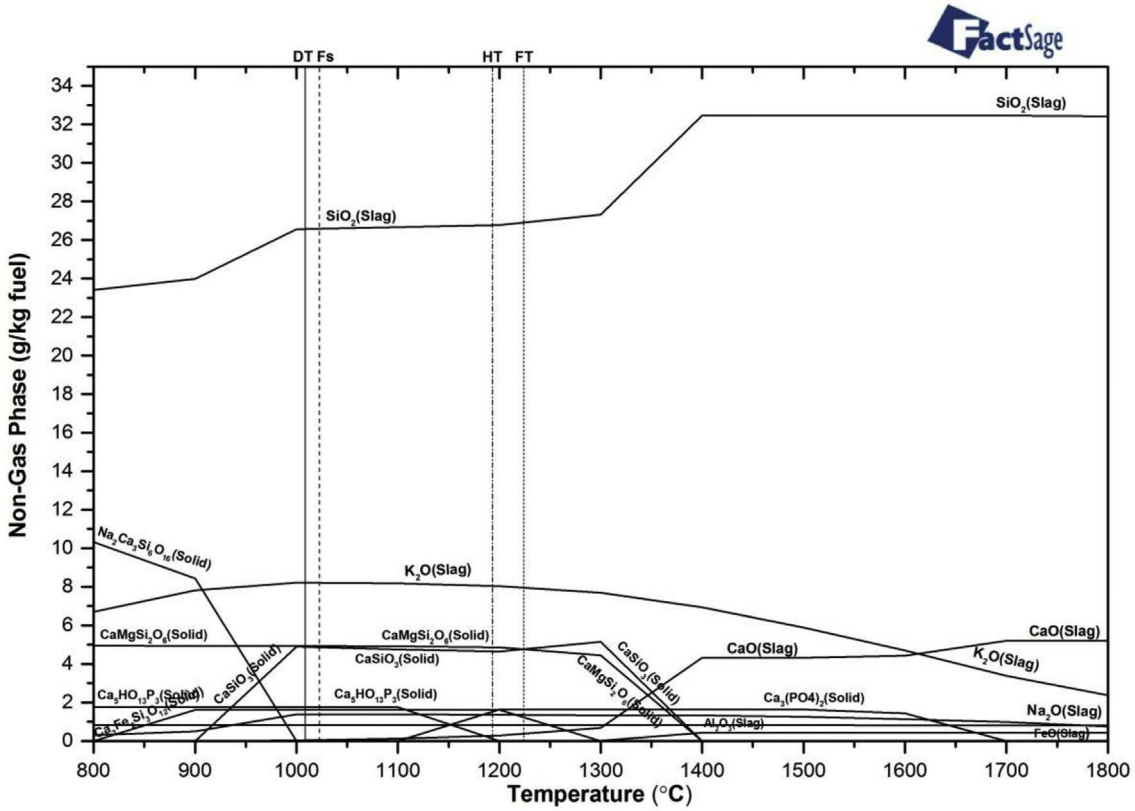

Fig. 7. Stable solid phases in equilibrium with the slag phase for 20% El Cerrejon coal 2 and 80% wheat straw co-combustion (BWCA82).

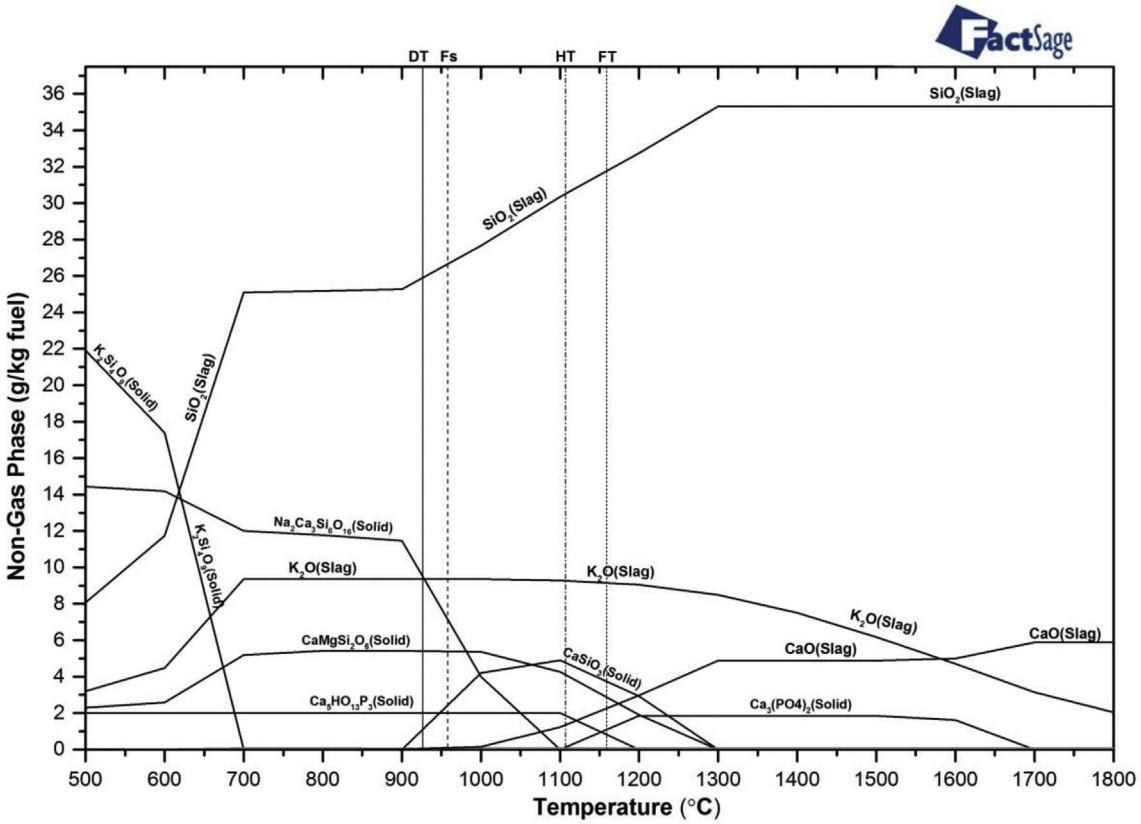

Fig. 8. Stable solid phases in equilibrium with the slag phase for 100% wheat straw (WS1).

Please cite this article in press as: P. Xing, et al., The use of equilibrium thermodynamic models for the prediction of inorganic phase changes in the co-firing of wheat straw with El Cerrejon coal, Journal of the Energy Institute (2018), https://doi.org/10.1016/j.joei.2018.02.003

$Ca_3Fe_2Si_3O_{12}(solid) \rightarrow CaO(slag) + FeO(slag) + SiO_2(slag)$ (>1300 °C)

When the wheat straw ratio increases from 20% to 80%, the main changes as shown by plots in Figs. 5–7 are listed as below:

$K_2Si_4O_9(solid) \rightarrow K_2O(slag) + SiO_2(slag)$ (>500 °C)

$Na_2Ca_3Si_6O_{16}(solid) \rightarrow Na_2O(slag) + CaSiO_3(solid)$ (900 °C)

$CaSiO_3(solid) \rightarrow CaO(slag) + SiO_2(slag)$ (>1100 °C)

The FactSage calculations showed good agreements with the XRD data for the presence of inorganic phases with temperature as shown in Tables 4 and 5. It also performed best over a wide range of fuel blends for the prediction of the slagging temperature, but tended to predict the on-set of slagging at a lower temperature than the deformation temperature measured by the ash fusion test. This might be expected, since there may be liquid phases beginning to form before there is any visual detection of changes in the ash during the ash fusion test.

The compositions of ash samples obtained from the pilot-scale test furnace were determined by XRD and the results are given in Table 6. Compared to the laboratory prepared ashes, fewer compounds were identified in the XRD of the pilot-scale test furnace ashes. Ashes obtained from the different locations within the combustor showed similar compositions in the XRD. The ashes were also reheated in the laboratory to 800 °C in order to burn off residual C-in ash. The XRD patterns of all of the fly ash, reheated fly ash, bottom ash, and reheated bottom ash were similar, with slightly better resolution in the reheated ashes, which resulted in the detection of $KAlSi_3O_8$. In Table 6 the XRD patterns were compared with results obtained by FactSage and good agreement was obtained.

4. Conclusions

The fusion temperatures and melting behaviour observed for the different ash samples were used to validate the FactSage model, which resulted in similar phase changes with temperature to the ones observed experimentally.

XRD measurements showed complex interactions between the inorganic species which changed with biomass type, blend ratio and temperature. Most inorganic phases present in the XRD tested results could be predicted by FactSage in the correct temperature range except the 20% El Cerrejon coal 2 with 80% wheat straw co-firing ash (BWCA82).

The FactSage model showed good agreement with XRD data for the presence of inorganic phases with temperature. For the coal and the wheat straw, and their blends, Factsage predicts that liquids begin to form at temperatures lower than the initial deformation temperature observed in the ash fusion test, and to increase in concentration up to the flow temperatures. The laboratory scale ashing experiments essentially quench the ash at different stages of mineral and slag transformations, and FACTSAGE performs well in the prediction of the mix of inorganic species present, at least qualitatively. It is therefore able to provide insight into the solid and liquid phases present as the ash heats, as well as the transformations it undergoes.

Acknowledgements

The authors acknowledge that the UKCCSRC PACT Facilities (funded by the Department for Business, Energy & Industrial Strategy and the Engineering and Physical Sciences Research Council) have been used for experimental work reported in this publication. The authors are grateful for financial support from Research Councils UK (Grant EP/K02115X/1). We wish to acknowledge the help of Dr A Lea-Langton with some of the XRD measurements.

Appendix A. Supplementary data

Supplementary data related to this article can be found at https://doi.org/10.1016/j.joei.2018.02.003.

References

[1] D. Bostrom, N. Skoglund, A. Grimm, C. Boman, M. Ohman, M. Brostrom, R. Backman, Ash transformation chemistry during combustion of biomass, Energy Fuels 26 (2012) 85–93.
[2] S.B. Hansen, P.A. Jensen, F.J. Frandsen, B. Sander, P. Glarborg, Mechanistic model for ash deposit formation in biomass suspension firing. Part 1: model verification by use of entrained flow reactor experiments, Energy Fuels 31 (2017) 2771–2789.
[3] S.B. Hansen, P.A. Jensen, F.J. Frandsen, B. Sander, P. Glarborg, Mechanistic model for ash deposit formation in biomass suspension firing. Part 2: model verification by use of full-scale tests, Energy Fuels 31 (2017) 2790–2802.
[4] Y. Niu, H. Tan, S. Hui, Ash-related issues during biomass combustion: alkali-induced slagging, silicate melt-induced slagging (ash fusion), agglomeration, corrosion, ash utilization, and related countermeasures, Prog. Energy Combust. Sci. 52 (2016) 1–61.
[5] M.U. Garba, D.B. Ingham, L. Ma, M.U. Degereji, M. Pourkashanian, A. Williams, Modelling of deposit formation and sintering for the co-combustion of coal with biomass, Fuel 113 (2013) 863–872.
[6] A. Grimm, N. Skoglund, D. Bostrom, D.M. Ohman, Bed agglomeration characteristics in fluidized quartz bed combustion of phosphorus-rich biomass fuels, Energy Fuels 25 (2011) 937–947.
[7] S.V. Vassilev, C.G. Vassileva, Y.-C. Song, W.-Y. Li, J. Feng, Ash contents and ash-forming elements of biomass and their significance for solid biofuel combustion, Fuel 208 (2017) 377–409.
[8] X. Wang, Y. Liu, H.Z. Tan, L. Ma, T. Xu, Mechanism research on the development of ash deposits on the heating surface of biomass furnaces, Ind. Eng. Chem. Res. 51 (2012) 12984–12992.
[9] Y.Q. Niu, H.Z. Tan, L. Ma, M. Pourkashanian, Z.N. Liu, Y. Liu, Slagging characteristics on the superheaters of a 12 MW biomass-fired boiler, Energy Fuels 24 (2010) 5222–5227.
[10] M. Reinmöller, M. Klinger, M. Schreiner, H. Gutte, Relationship between ash fusion temperatures of ashes from hard coal, brown coal, and biomass and mineral phases under different atmospheres, A combined FactSage™ computational and network theoretical approach, Fuel 151 (2015) 118–123.
[11] W. Bale, E. Bélisle, P. Chartrand, S.A. Decterov, G. Eriksson, A.E. Gheribi, K. Hack, I.-H. Jung, Y.-B. Kang, J. Melançon, A.D. Pelton, S. Petersen, C. Robelin, J. Sangster, P. Spencer, M.-A. Van Ende, FactSage thermochemical software and databases, 2010–2016, CALPHAD 54 (2016) 35–53.
[12] T. Rizvi, P. Xing, M. Pourkashanian, L.I. Darvell, J.M. Jones, W. Nimmo, Prediction of biomass ash fusion behaviour by the use of detailed characterisation methods coupled with thermodynamic analysis, Fuel 141 (2015) 275–284.

Please cite this article in press as: P. Xing, et al., The use of equilibrium thermodynamic models for the prediction of inorganic phase changes in the co-firing of wheat straw with El Cerrejon coal, Journal of the Energy Institute (2018), https://doi.org/10.1016/j.joei.2018.02.003

[13] P. Xing, L.I. Darvell, J.M. Jones, L. Ma, M. Pourkashanian, A. Williams, Experimental and theoretical methods for evaluating ash properties of pine and El Cerrejon coal used in co-firing, Fuel 183 (2016) 39–54.
[14] P. Xing, P. Mason, S. Chilton, S. Lloyd, J.M. Jones, A. Williams, W. Nimmo, A comparative assessment of X-ray fluorescence and wet chemical analysis methods for ash composition analysis of solid biomass fuels, Fuel 182 (2016) 161–165.
[15] J.D. Watt, The flow properties of slag formed from the ashes of British coals: Part 2: the crystallizing behaviour of the slags, J. Inst. Fuel 42 (1969) 131–134.
[16] M.S. Oh, D.D. Brooker, E.F. DePaz, J.J. Brady, T.R. Decker, Effect of crystalline phase formation on coal slag viscosity, Fuel Process. Technol. 44 (1995) 191–199.
[17] Y. Niu, Y. Zhu, S. Hui, J.M. Jones, Y. Liu, A calculation method of biomass rate based on crystallization theory, Asia Pac. J. Chem. Eng. 9 (2014) 456–463.
[18] A.G. Clements, S. Black, J. Szuhánszki, K. Stępchły, A. Pranzitelli, W. Nimmo, M. Pourkashanian, LES and RANS of air and oxy-coal combustion in a pilot-scale facility: predictions of radiative heat transfer, Fuel 151 (2015) 146–155.
[19] A.R. McLennen, G.W. Bryant, C.W. Bailey, B.R. Stanmore, T.F. Wall, Index for iron-based slagging for pulverized coal firing in oxidizing and reducing conditions, Energy Fuels 14 (2000) 349–354.

Please cite this article in press as: P. Xing, et al., The use of equilibrium thermodynamic models for the prediction of inorganic phase changes in the co-firing of wheat straw with El Cerrejon coal, Journal of the Energy Institute (2018), https://doi.org/10.1016/j.joei.2018.02.003